Gait Phase Estimation in Steady Walking: A Comparative Study of Methods Based on the Phase Portrait of the Hip Angle

Ali Reza Manzoori[1], Tian Ye[1], Davide Malatesta[2], Coline Lugaz[3], Olivier Pajot[3], Auke Ijspeert[1] and Mohamed Bouri[1]

***Abstract*— Accurate real-time estimation of the gait phase (GP) is crucial for many control methods in exoskeletons and prostheses. A class of approaches to GP estimation construct the phase portrait of a segment or joint angle, and use the normalized polar angle of this diagram to estimate the GP. Although several studies have investigated such methods, quantitative information regarding their performance is sparse. In this work, we assess the performance of 3 portrait-based methods in flat and inclined steady walking conditions, using quantitative metrics of accuracy, repeatability and linearity. Two methods use portraits of the hip angle versus angular velocity (AVP), and hip angle versus integral of the angle (IAP). In a novel third method, a linear transformation is applied to the portrait to improve its circularity (CSP). An independent heel-strike (HS) detection algorithm is employed in all algorithms, rather than assuming HSs to occur at a constant point on the portrait. The novel method shows improvements in all metrics, notably significant root-mean-square error reductions compared to IAP (-3%, $p < 0.001$) and AVP (-2.4%, $p < 0.001$) in slope, and AVP (-1.61%, $p = 0.0015$) in flat walking. A non-negligible inter-subject variability is observed between phase angles at HS (equivalent to up to 8.4% of error in the GP), highlighting the importance of explicit HS detection for portrait-based methods.**

I. INTRODUCTION

Progress in the Gait Cycle (GC) is usually quantified by a number starting from 0 Heel-Strike (HS) and linearly increasing to 1 at the next ipsilateral HS. This parameterization of the GC, also known as "Gait Phase (GP)" or "percent gait cycle", is useful in various applications, both in analysis (e.g., gait assessment) and synthesis (e.g., control of exoskeletons and prostheses), since it facilitates comparison and generalization of profiles across gaits, independent from the duration. For gait analysis this value is typically calculated post hoc, by normalizing the time elapsed since HS over the GC duration. For synthesis applications, however, calculating the instantaneous value of the GP is often necessary in real-time, which is not trivial since it requires an exact knowledge of the duration of the current GC before it ends.

Numerous methods have been proposed for the real-time estimation of the GP. The basic approach is to detect the HS and normalize the elapsed time since this event over an estimated duration of the GC, which can either be assumed to be a constant [1] or equal to the average duration of the recent strides [2]. While under controlled conditions such as walking on a treadmill at a steady pace, these methods can provide a good estimation, they are not reliable in more realistic scenarios where the GC duration varies.

In another approach, adaptive frequency oscillators (AFOs) are used to calculate the GP [3], [4]. Thanks to the continuous estimation of the gait frequency by the AFO, these methods can handle pace variations; however, in case of rapid changes or a continuously fluctuating pace, the convergence rate of the AFO might not be sufficient to keep the synchronization. Data-driven and machine-learning-based methods have also been utilized to estimate the GP [5], [6], but the accuracy of these methods is dependent on their training, and hence their performance is not guaranteed for gaits they have not been trained for.

Other methods inspired by the legged robotics literature attempt to find a state variable of the system that inherently captures progression in the GC, referred to as a "phase variable" [7]. By relying directly on the instantaneous changes of the phase variable, these methods have the potential to swiftly adapt to changes in pace and even sudden perturbations of gait such as stumbling [8], without the need for a learning/adaptation period or gait-specific tuning. In order to uniquely represent the GC progression at each instant, a phase variable should be strictly monotonic over each cycle. A commonly used phase variable is the polar angle of the Phase Portrait (PP) plot constructed from a joint or segment angle as input [9]. Because of the periodicity of gait, these PPs form closed curves; thus, with an appropriate choice of the input, the polar angle of the portrait satisfies the monotonicity requirement.

Numerous studies have investigated the performance of PPs constructed from different input variables in terms of properties such as linearity and piece-wise-monotonicity [9], or robust parameterization of the kinematics under walking perturbations [8], [10] and in different walking conditions [11]. However, the GP estimation performance of these methods has rarely been directly assessed. Furthermore, the start of the GC (i.e. the HS event) has commonly been assumed to occur at a constant polar angle in previous works [12], but a recent study has suggested that this assumption can lead to errors of up to about 20% [13].

In this article, three phase-portrait-based approaches to GP estimation using the hip flexion/extension angle ("hip

*AM received funding from the European Union's Horizon 2020 research and innovation programme under the Marie Sklodowska-Curie Grant Agreement No. 754354.

[1]AM, TY, AI & MB are with the Biorobotics Laboratory (BioRob) of EPFL, 1015 Lausanne, Switzerland. {ali.manzoori, tian.ye, auke.ijspeert, mohamed.bouri}@epfl.ch

[2]DM is with the Institute of Sport Sciences (ISSUL) of UNIL, 1015 Lausanne, Switzerland. davide.malatesta@unil.ch

[3]CL and OP are with the Innovation, Incubation & Investment Cell (i3@EPFL) of Sonceboz, 2605 Sonceboz-Sombeval, Switzerland. {coline.lugaz, olivier.pajot}@sonceboz.com

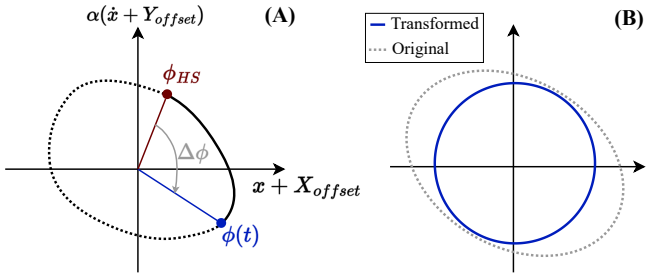

Fig. 1. (A) Illustration of the PP used to estimate the GP. Note that the polar radius of the curve rotates clockwise. (B) Applying a stretching transformation to the original PP to make it more circular.

angle" for short) are compared. The choice of hip angle was motivated by previous results showing its suitability (in terms of monotonic and linear behavior) for the PP methods [8]. In the first approach, the portrait is constructed from the hip flexion/extension angle and its time derivative (angular velocity), while in the second approach the PP is generated from the hip angle and its integral. Using the integral in the second approach is inspired by past studies highlighting the improved linearity of its response [10]. In the third approach, a novel modification is applied to the PP to reduce its ellipticity. A systematic assessment of the quality of GP estimation using these methods is performed in terms of accuracy, repeatability, and linearity. We hypothesize that the second method will offer better accuracy compared to the first, and that the novel method will outperform the first two. Furthermore, we examine the assumption of a constant polar angle at HS by checking the distribution of polar angles at the moments of HS.

II. METHODS

A. GP Estimation

The first step in phase-portrait-based approaches to the estimation of the GP is to construct a PP, which consists of a plot representing a state variable, x, against its time-derivative, $\dot{x}$. Due to the periodicity of gait, this PP will form a closed curve. By adding offsets to x and $\dot{x}$ to zero-center them, the closed curve will encircle the origin and therefore its polar radius will cover a full orbit over each GC. Thus, by normalizing the angle traversed since the moment of HS over 2π rad, the GP (p_{GC}) can be estimated as a continuous value in the 0–1 range:

$$p_{GC}(t) = \frac{|\phi(t) - \phi_{HS}|}{2\pi} \tag{1}$$

where $\phi(t)$ is the instantaneous polar angle of the PP, and ϕ_{HS} is the polar angle at which the last ipsilateral HS occurred (Fig. 1A). To reduce the ellipticity of the closed curve, $\dot{x}$ is linearly scaled so as to have a similar range to x. Reducing the ellipticity decreases the variation in the traversed polar angle ϕ given a constant traversed arc length on the PP, which results in a more linear estimated GP. The zero-centering offsets for x and $\dot{x}$ and the scaling factor are respectively calculated as:

$$X_{offset} = -\frac{x_{Max} + x_{min}}{2} \tag{2}$$

$$Y_{offset} = -\frac{\dot{x}_{Max} + \dot{x}_{min}}{2} \tag{3}$$

$$\alpha = \frac{x_{Max} - x_{min}}{\dot{x}_{Max} - \dot{x}_{min}} \tag{4}$$

where x_{Max} and $\dot{x}_{Max}$ are the upper bounds of x and $\dot{x}$ respectively, and x_{min} and $\dot{x}_{min}$ are their lower bounds.

The fundamental approach explained above is common to all of the phase-portrait-based estimation methods presented in the literature and studied in this work. The differences between individual methods lie in the details of PP construction. These details are described below for the methods investigated in this article.

1) Angle-Velocity Portrait (AVP) method: In the first approach tested in this study, x is considered to be the hip angle, θ_h, and $\dot{x}$ is the hip angular velocity, $\dot{\theta}_h$. Since in practice $\dot{\theta}_h$ is estimated via numerical differentiation of the hip angle sampled at a high rate, it is prone to high-frequency noise. Therefore, it is low-pass-filtered using a first-order IIR filter ($f_c = 1.6$ Hz) before construction of the PP. Note that the delay induced by the filter would distort the circularity of the PP if it were a perfect circle, but here the distortion is not expected to have a significant effect since the PP is already elliptical.

2) Integral of angle-Angle Portrait (IAP) method: In addition to high-frequency noise, the $\dot{\theta}_h$ signal itself can have short-term oscillatory behavior, notably at the moment of HS due to the impact with the ground. These short-term oscillations lead to non-monotonic behavior of ϕ and therefore errors in GP estimation. To reduce the effect of such oscillations, in the second approach we use $\int \theta_h dt$ and θ_h as x and $\dot{x}$, respectively. Due to the inherent smoothing caused by integration, the local oscillations are damped. To remove the constant drift of $\int \theta_h dt$, it is high-pass filtered (first-order IIR, $f_c = 1$ Hz) prior to constructing the PP.

3) Circular Shaped Portrait (CSP) method: Despite the re-scaling of $\dot{x}$ to enforce a similar range on the horizontal and vertical axes, the PP is still not circular due to θ_h not having a perfectly sinusoidal profile. The ellipsoidal shape of the PP induces variability in the rate of change of ϕ over the course of a cycle, resulting in a nonlinear estimation of GP. In this approach, we apply a stretching transformation to the PP to further reduce its ellipticity (Fig. 1B), using a linear transformation operation according to

$$\begin{pmatrix} x_T \\ \dot{x}_T \end{pmatrix} = T \begin{pmatrix} x \\ \dot{x} \end{pmatrix} \tag{5}$$

where T is the 2×2 transformation matrix, and the subscript $_T$ denotes the transformed PP coordinates. Based on previous observations, it was known that the PP are more stretched along the $X = Y$ diagonal. Therefore, we considered T to be a general stretching matrix along $X = -Y$, defined as:

$$T = 0.5 \times \begin{bmatrix} 1+k & 1-k \\ 1-k & 1+k \end{bmatrix} \tag{6}$$

where $k > 1$ determines the magnitude of stretching. In this study, we chose $k = 2.3$ by visually checking the circularity of the transformed PPs obtained in a pilot experiment with one subject walking at the same conditions as our final protocol. Note that the isotropic scaling by this matrix does not have any effects on the GP estimation, since the polar angle is invariant under such scaling. The same variables as the IAP method were used as x and $\dot{x}$, on which the transformation was applied. To the best of our knowledge, this method has not previously been introduced in the literature.

As mentioned in the introduction, ϕ_{HS} has typically been assumed to be constant in past studies using this method. However, due to the natural variations in the gait pattern,we hypothesize that HS can happen at different angles. In this study, we detect the HS events and update ϕ_{HS} in each GC. The HS detection algorithm first detects the landing preparation sub-phase of the swing leg from the zero-crossing of the ipsilateral hip angular velocity, and then detects the HS when the vertical trunk acceleration goes above $1.2\,\mathrm{m\,s^{-2}}$ due to the impact with the ground. The thresholds were experimentally found in pilot tests with 5 subjects walking on the treadmill at slow, medium and fast speeds.

B. Experimental Protocol and Setup

A hip exoskeleton (e-Walk V1) was used for measurement and real-time estimation. The device is attached to the wearer at the waist and the thighs, using orthotic attachments (Fig. 2A). Two BLDC motors with a 6:1 planetary reducer mounted directly on the waist attachment actuate the hip joints in the sagittal plane. The outputs of the motors are connected to the thigh attachments via thin rectangular segments made of carbon-fiber-reinforced polymer. The flexibility of these segments in the transverse direction provides a passive degree of freedom in the frontal plane, to avoid blocking the abd/adduction in the range required for normal walking. The encoders of the actuators measure the hip angles. Due to the efficient and low-ratio reducers, the motors could be easily back-driven by the wearer (back-driving torque $< 0.6\,\mathrm{N\,m}$ RMS for movements of up to $2\,\mathrm{Hz}$). The exoskeleton is also equipped with an IMU (located near the lower-back) and a pair of insole force sensors. The embedded computer of the exoskeleton (BeagleBone Black, BeagleBoard.org Foundation, USA) performed the processing and GP estimation. All electronics and batteries are on-board, and the total weight of the exoskeleton is $5\,\mathrm{kg}$. Data acquisition from all of the sensors, calculation of the GP values, and data logging were performed at $500\,\mathrm{Hz}$.

Twenty healthy adults (3 females, 17 males; age: 21–59 years old, mean: 28.8 ± 9.3 years) participated in this study. All subjects provided informed consent before participating in the experiment. The protocol was approved by the local ethics committee of the canton of Vaud (CER-VD).

The subjects donned the exoskeleton and walked on a single-belt treadmill (T150-FMT-MED, Arsalis, Belgium) installed on a custom tilt platform for adjusting the inclination (Fig. 2B). Two walking conditions were tested, both at a constant speed of $1.1\,\mathrm{m\,s^{-1}}$ and a duration of $5\,\mathrm{min}$: *(i)* treadmill at 0% inclination (condition Flat or -F), and *(ii)* treadmill at an upward inclination of 10% (condition Slope or -S). The first 15 seconds of walking in each condition were used to calibrate the values of X_{offset}, Y_{offset}, and α (defined in Eqs. 2–4). The order of conditions was randomized between the subjects. The GP estimation using the three methods was performed in parallel on the embedded computer of the exoskeleton.

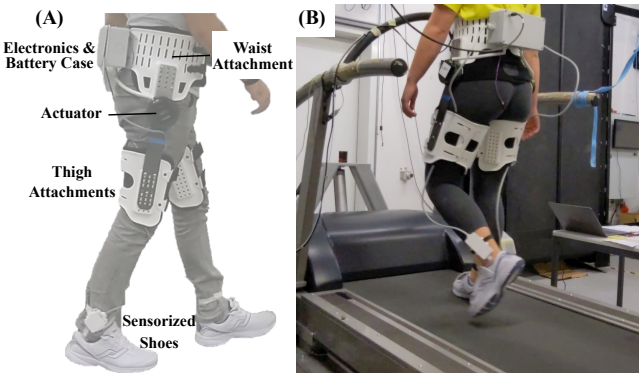

Fig. 2. The hip exoskeleton used for the measurement and estimation (A) and the experimental setup (B).

C. Data analysis

Data analysis was performed using MATLAB (Mathworks Inc., USA). Data for each subject was segmented into single GCs based on the HSs detected during the experiment, which were also validated against the foot load signals. The first and last 10 strides of each condition were discarded from the analysis to ensure steady-state walking. The segmentation was performed separately for each leg based on the ipsilateral HSs, but since the results were symmetric, only the left side was used in the analysis. The true GP for each cycle was calculated by normalizing the time since HS over the entire duration of that GC and used as the ground truth for error calculations. The following metrics were used for performance assessment:

1) Root-Mean-Square Error (RMS-E): This metric, which serves as a measure of accuracy, was calculated as the RMS value of the error between the average GP profile (calculated over all subjects and strides) of each method and the true GP.

2) RMS Standard Deviation (RMS-SD): This metric characterizes the overall repeatability or variation in the GP profiles estimated by each method for a given subject. It was first calculated for each subject individually, by taking the RMS value of the standard deviation of the single-stride GP profiles. Then, the average was calculated over all subjects.

3) Mean Linearity (r_{mean}): The Pearson correlation coefficient (r) was used as a metric of the linearity of the profiles. The coefficient was first calculated between the estimated and true GP for each single stride, and then the average value was calculated over all strides and subjects.

Differences in metrics were tested for statistical significance by comparing the subject means between different methods within each condition (Flat or Slope) using a

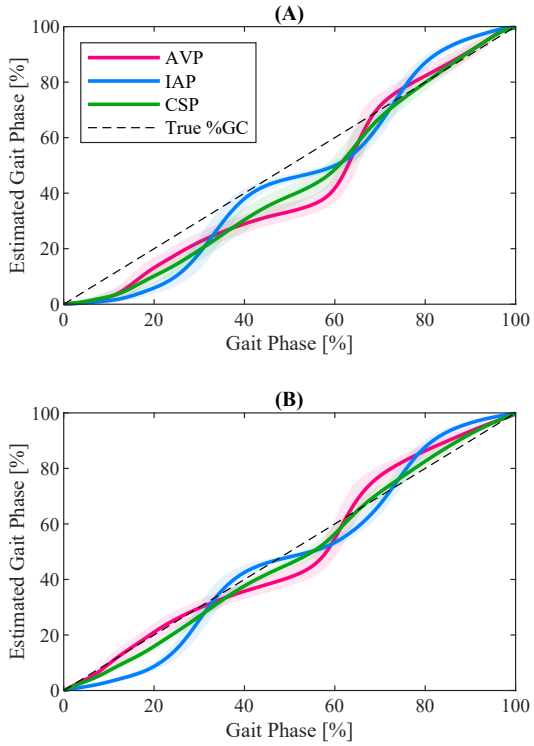

Fig. 3. Mean estimated GP profiles for walking for the two conditions: (A) Flat, (B) Slope. The shaded area around each line marks the standard deviation of the profile.

repeated measures one-way ANOVA, followed by post-hoc testing using Wilcoxon's matched pairs signed rank test if needed.

III. RESULTS

A. Estimated GP Profiles

The average estimated GP profiles for all methods are shown in Fig. 3 and the performance metrics are presented in Table I. The pairwise differences in performance between the methods within each condition were significantly different in terms of all metrics ($p < 0.05$), except for RMS-E between IAP and CSP in Flat ($p = 0.33$), and RMS-SD between AVP and IAP in Flat ($p = 0.23$). Overall, the performance of the GP estimation for all of the methods was better in terms of accuracy, repeatability and linearity in the Slope condition. The CSP method outperformed AVP and IAP in both conditions according to all of the metrics. Between the other methods, IAP had a better linearity score in both conditions, whereas in terms of accuracy and repeatability it was only superior in the Flat condition.

B. HS Phase Angles

Since the PPs of the IAP and CSP methods only differ in a linear transformation (inducing a slight shift in the phase angle at HS), only the results of the AVP and IAP methods are presented. The distribution of the mean phase angles at HS between subjects are presented in Fig. 4A, showing the inter-subject differences. As an example of the intra-subject differences, the distribution of phase angles over

TABLE I

METRICS OF ACCURACY, REPEATABILITY AND LINEARITY OF THE ESTIMATED GP FOR THE THREE METHODS. PAIRS OF METRICS THAT ARE NOT SIGNIFICANTLY DIFFERENT HAVE BEEN MARKED WITH AN IDENTICAL SUPERSCRIPT.

Method	Condition	RMS-E	RMS-SD	$\mathbf{r_{mean}}$
AVP	**Flat (F)**	9.70	$1.97^{\boxminus}$	0.9779
	Slope (S)	5.78	1.74	0.9861
IAP	**Flat (F)**	8.42^{-}	$1.91^{\boxminus}$	0.9867
	Slope (S)	6.40	1.90	0.9892
CSP	**Flat (F)**	8.09^{-}	1.67	0.9907
	Slope (S)	3.40	1.58	0.9971

different strides of the same subject are also presented for a representative participant in Fig. 4B. The distributions show a non-negligible variation in the phase angles at HS on both inter- and intra-subject levels. When normalized, the inter-subject differences in ϕ_{HS} lead to a maximum error of 8.41% (AVP-F), 3.98% (IAP-F), 6.78% (AVP-S), and 2.60% (IAP-S) in GP estimation between the subjects. Similarly, the intra-subject differences in ϕ_{HS} for the representative participant can produce a maximum error of 7.93% (AVP-F), 2.75% (IAP-F), 0.77% (AVP-S), and 1.14% (IAP-S).

C. Phase Portraits

The general trends between the PPs generated by the three methods in Flat and Slope conditions were qualitatively similar for each subject, but some marked distinctions existed across subjects due to the inter-individual differences in gait pattern. Hence, rather than the average PPs across subjects, we present the PPs averaged over the strides of one representative subject (Figs. 4C and 4D), which is more indicative of the real shape of the single-stride portraits. As expected, the AVP and IAP portraits have a more elliptic shape, whereas the CSP portrait is more circular, thanks to the stretching transformation.

IV. DISCUSSION

A. Overall Estimation Quality

Our results show that all of the three methods are capable of estimating the GP in real-time with varying levels of accuracy (RMS-E of less than 10% in the worst and less than 4% in the best case), corroborating the general suitability of the hip angle as a phase variable for parameterizing the GC.

Even though the error levels remain relatively low on average, none of the methods give a perfectly linear estimation due to the deviation of the PPs from perfect circularity. This also causes considerable local errors, most noticeable in the late stance phase ($\sim 60\%$ of the GC) of the estimated GP by the AVP method for Flat (Fig. 3A). Intuitively, this can be explained by the fact that each of the stance and swing periods geometrically cover half of the PP, while temporally they account for 60% and 40% of the GC, respectively. This discrepancy between the geometrical and temporal proportions of the phases results in a lower rate of change of the estimated GP in the stance phase. However, the repeatability of the shape of the estimated profiles for each

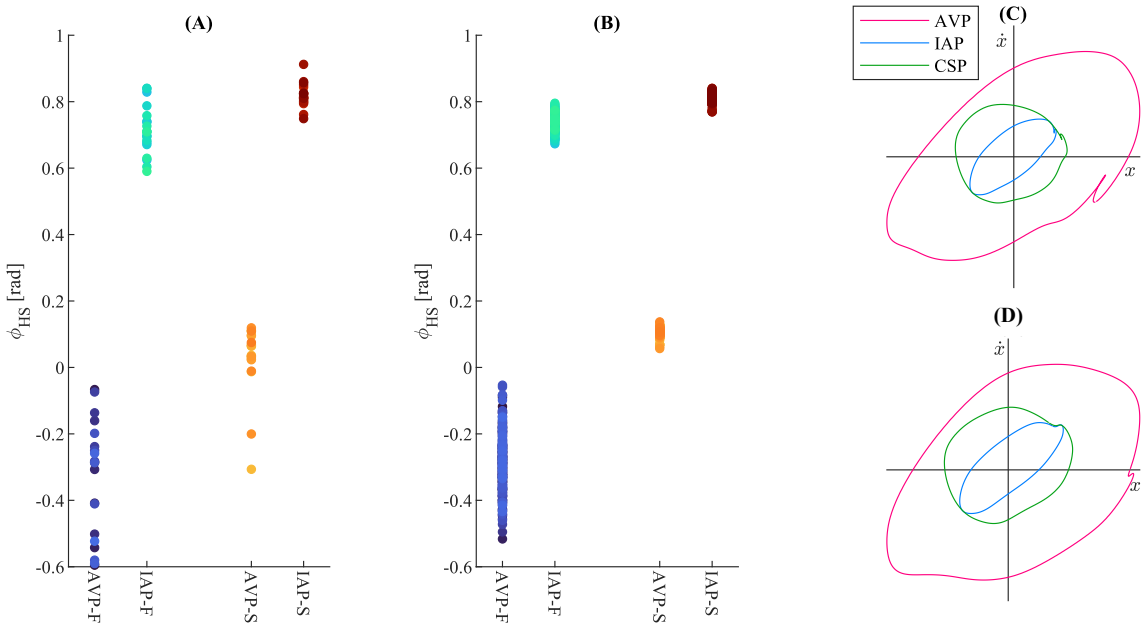

Fig. 4. Phase angles at HS and PPs for the different methods and conditions. (A) Distribution of the average phase angles at HS between all of the subjects. (B) Distribution of the phase angles at HS between different strides for one subject. (C) Average PPs generated by each method for one subject in the Flat condition. (D) Average PPs generated by each method for one subject in the Slope condition. Note that in (C) and (D), the shapes have been arbitrarily scaled (isotropically) for better visibility. Also, flexion was taken to be the positive direction for the hip angle.

method (indicated by a narrow band of standard deviation around the profiles in Fig. 3) suggests that using a constant nonlinear mapping to generate a more linear estimation could be feasible.

B. Comparison among Methods

The novel method presented in this work (CSP) showed a clear improvement in the estimation performance in all aspects of accuracy, repeatability and linearity. This improvement in the performance is due to the more circular shape of the PP, as can be observed in Fig. 4C–D. It is worth noting that the transformation matrix was found heuristically in this study; a more data-driven or analytical approach to the design of the transformation matrix is likely to bring about further improvements.

Between the two other methods, AVP has a more irregular behavior in terms of accuracy; that is, in some regions it is very accurate (e.g., during mid- to late-swing in Flat, and early- to mid-stance in Slope), while in others it has a marked deviation from the true GP. The IAP method, in contrast, has a more uniform behavior in terms of error, due to fewer anomalies in the shape of its PP. On the other hand, the more elliptic shape of the IAP portrait leads to a quasi-periodic increase and decrease in the slope of its estimated GP profile.

C. Comparison among Conditions

All of the methods had a better performance in Slope in all metrics. This difference can mostly be attributed to a smoother behavior around HS in the Slope condition, which was also evidenced by markedly less oscillatory behavior of the hip angular velocity signal observed during data analysis. This is also seen in the reduced variance of the HS phase angles in Slope (see section IV-D). As can be seen by comparing Figs. 3A and 3B, the main difference between Flat and Slope profiles is due to the relatively constant portion in the first 10% of the GC in the Flat condition, creating a lag in the profiles. This results from the nonsmooth shape of the PP after HS, which can sometimes even lead to a momentarily non-monotonous behavior of the phase angle (for a clear example, see the knot in the 4^{th} quadrant of the AVP profile in Fig. 4C). Lastly, the notable difference in performance between Flat and Slope emphasizes the importance of testing gait detection and estimation algorithms under different walking conditions.

D. Distribution of HS Phase Angles

As demonstrated in Fig. 4A–B, the variability in the phase angles at HS on both the intra- and inter-subject levels is non-negligible. Part of the intra-subject variability is due to small variations in the timing of HS detection (on the order of tens of milliseconds) with respect to the moment of impact between different strides. Due to the jerky behavior around impact, even small differences in timing in this period can sometimes lead to noticeable differences in the phase angle. This is evidenced by the fact that intra-subject variability is higher in Flat, since the impact is stronger in this condition as explained in IV-C. The angular velocity signal is especially susceptible to oscillations caused by the impact due to the amplifying effect of differentiation, which explains the highest intra-subject variability occurring in AVP-Flat (AVP-F in Fig. 4B). Inter-subject variations, on the other hand, are more attributable to actual differences in gait pattern, which

was also observed in the inter-individual distinctions in PP shapes. The range of variation between subjects was also more significant than between the strides of the same subject. Therefore, while the assumption of a constant phase angle for HS might be acceptable for each subject, this assumption is not likely to be generalizable among different individuals.

E. Implications for the Control of Assistive Devices

Since one of the main applications of real-time GP estimation is for the control of assistive devices, it is worth paying special attention to the ramifications of our findings for this use case. First, it was observed that even though the overall estimation of the GP is fairly accurate, local errors of up to around 20% can occur, particularly with the AVP method. This suggests that care must be taken when feeding the estimated GP from this method as an input to a position or torque profile (which is the most common use case control). For example, a torque profile consisting of a narrow burst at late stance or early swing might be severely distorted as a result of the local errors in GP.

Another important observation is the sensitivity of these methods to impacts, manifested by the challenges due to HS as discussed in sections IV-C and IV-D. This implies that using these methods in conjunction with torque or movement profiles that include abrupt changes can induce undesirable interaction effects between the assistance and the GP estimation. This is particularly likely if the hip joint is directly affected by the control action.

F. Limitations

The main limitation of this work is the fact that only one walking speed was tested, which was due to time constraints for carrying out the experiments. Therefore, no direct conclusions about the effect of walking speed on the estimation performance can be drawn. Furthermore, we only studied steady-state treadmill walking in this work, in order to facilitate a systematic comparison. However, for a more realistic assessment of the estimation quality, non-steady overground walking with variable speeds, cadences and terrains should also be studied. Finally, our sample only included healthy and mostly young adults. It could be of interest, particularly for more rehabilitation-oriented applications, to also test the estimation performance with persons with gait impairments and also older individuals, since there might be systematic differences in their gait patterns compared to the young and able-bodied population.

V. CONCLUSION

We presented a novel phase-portrait-based GP estimation method using a stretching transformation to improve portrait circularity, and compared this method against conventional portrait-based approaches by evaluating the estimation according to quantitative metrics. Our method showed a significantly improved estimation performance in terms of accuracy, repeatability and linearity. The results also provide insight into general strengths and limitations of the different portrait-based methods. Different levels of accuracy were observed depending on the subphases of the GC. All methods performed remarkably better in inclined walking. The main challenge was identified to be the sensitivity of these methods to impact and jerky behavior. Lastly, our results highlight the importance of explicit HS detection in portrait-based methods.

ACKNOWLEDGMENT

We would like to express our sincere gratitude to: Dr. Romain Baud for his help in preparing the software and hardware of the exoskeleton, Olivier Clerc for his assistance in the experiments and data analysis, Julia Primavesi and Sara Messara for their assistance in carrying out the experiments, Jérôme Parent for his help in preparing the experimental setup, and all of the subjects for their time and participation.

REFERENCES

[1] A. J. Young, J. Foss, H. Gannon, and D. P. Ferris, "Influence of power delivery timing on the energetics and biomechanics of humans wearing a hip exoskeleton," *Frontiers in Bioengineering and Biotechnology*, vol. 5, 2017.

[2] C. L. Lewis and D. P. Ferris, "Invariant hip moment pattern while walking with a robotic hip exoskeleton," *Journal of Biomechanics*, vol. 44, no. 5, pp. 789–793, Mar. 2011.

[3] K. Seo, S. Hyung, B. K. Choi, Y. Lee, and Y. Shim, "A new adaptive frequency oscillator for gait assistance," in *2015 IEEE International Conference on Robotics and Automation (ICRA)*, May 2015, pp. 5565–5571.

[4] T. Yan, A. Parri, V. Ruiz Garate, M. Cempini, R. Ronsse, and N. Vitiello, "An oscillator-based smooth real-time estimate of gait phase for wearable robotics," *Autonomous Robots*, vol. 41, no. 3, pp. 759–774, Mar. 2017.

[5] I. Kang, P. Kunapuli, and A. J. Young, "Real-time neural network-based gait phase estimation using a robotic hip exoskeleton," *IEEE Transactions on Medical Robotics and Bionics*, vol. 2, no. 1, pp. 28–37, Feb. 2020.

[6] M. Shushtari, H. Dinovitzer, J. Weng, and A. Arami, "Ultra-robust real-time estimation of gait phase," *IEEE Transactions on Neural Systems and Rehabilitation Engineering*, vol. 30, pp. 2793–2801, 2022.

[7] R. D. Gregg, E. J. Rouse, L. J. Hargrove, and J. W. Sensinger, "Evidence for a time-invariant phase variable in human ankle control," *PLOS ONE*, vol. 9, no. 2, p. e89163, Feb. 2014.

[8] D. J. Villarreal, H. A. Poonawala, and R. D. Gregg, "A robust parameterization of human gait patterns across phase-shifting perturbations," *IEEE Transactions on Neural Systems and Rehabilitation Engineering*, vol. 25, no. 3, pp. 265–278, Mar. 2017.

[9] D. J. Villarreal and R. D. Gregg, "A survey of phase variable candidates of human locomotion," in *2014 36th Annual International Conference of the IEEE Engineering in Medicine and Biology Society*, Aug. 2014, pp. 4017–4021.

[10] ——, "Unified phase variables of relative degree two for human locomotion," in *2016 38th Annual International Conference of the IEEE Engineering in Medicine and Biology Society (EMBC)*, Aug. 2016, pp. 6262–6267.

[11] R. Macaluso, K. Embry, D. J. Villarreal, and R. D. Gregg, "Parameterizing human locomotion across quasi-random treadmill perturbations and inclines," *IEEE Transactions on Neural Systems and Rehabilitation Engineering*, vol. 29, pp. 508–516, 2021.

[12] D. Quintero, D. J. Lambert, D. J. Villarreal, and R. D. Gregg, "Real-time continuous gait phase and speed estimation from a single sensor," in *2017 IEEE Conference on Control Technology and Applications (CCTA)*, Aug. 2017, pp. 847–852.

[13] R. Nasiri, H. Dinovitzer, and A. Arami, "A unified gait phase estimation and control of exoskeleton using virtual energy regulator (ver)," in *2022 International Conference on Rehabilitation Robotics (ICORR)*, Jul. 2022, pp. 1–6.